Ocean Engineering 46 (2012) 9–17

Contents lists available at SciVerse ScienceDirect

Ocean Engineering

journal homepage: www.elsevier.com/locate/oceaneng

Comparison study of a pusher–barge system in shallow water, medium shallow water and deep water conditions

K.K. Koh [a,*], H. Yasukawa [b]

[a] Faculty of Mechanical Engineering, Universiti Teknologi Malaysia, 81310 Skudai, Johor, Malaysia
[b] Graduate School of Engineering, Hiroshima University, 1-4-1 Kagamiyama, Higashi Hiroshima 739-8527, Japan

ARTICLE INFO

Article history:
Received 24 March 2011
Accepted 3 March 2012
Editor-in-Chief: A.I. Incecik
Available online 22 March 2012

Keywords:
Pusher–barge
Shallow water condition
Turning motion
Maneuvering simulation
Rotating arm test

ABSTRACT

The study of pusher–barge system in this paper is a continuation research of nine different pusher–barge systems and eight unconventionally arranged pusher–barge systems (Yasukawa et al., 2007; Koh et al., 2008a,b). In this study, pusher–barge system with one pusher and one barge arranged in a linear combination (11*BP*) was brought into shallow water condition and tested at Kyushu University, Japan with water height to ship draught ratio (h/d): 1.2 (shallow water); 1.5 (medium shallow water); and 19.3 (deep water) conditions. Least squares' fitting method was used in determining the hydrodynamic derivatives that are suitable for the three water draught ratio conditions. Linear derivatives from the experiments were compared with studies from different researchers (Fujino and Ishiguro, 1984; Yoshimura, 1986; Yoshimura and Sakurai, 1989). Added mass was calculated using singularity distribution method under the assumption of rigid free surface. Propeller and rudder hull interaction parameters were pre-assumed based on the study of other researchers. In the study, negative course stability was found in shallow water condition (unstable in course keeping). Maneuvering simulations at 20° and 35° turning show that pusher–barge 11*BP* has the largest turning circle in deep water condition and smallest turning circle in shallow water condition. Course keeping ability decreases from deep water to medium shallow water to shallow water conditions.

1. Introduction

As a continuous study to the nine different pusher–barge systems (Yasukawa et al., 2007; Koh et al., 2008a) and eight unconventionally arranged pusher–barge systems (Koh et al., 2008b), pusher–barge 11*BP* was brought into shallow water condition and its maneuvering performance in shallow water condition was compared with medium shallow water and deep water conditions. Since pusher–barge systems are often being operated in inland waterway with limited water depth, hence the study of pusher–barge system in shallow water condition brings a more realistic scene of how the pusher–barge will perform in real life.

Shallow water rotating arm tests of pusher–barge 11*BP* were conducted at Kyushu University, Japan in the study. Hydrodynamic derivatives were obtained by least squares fitting to the model test data. Maneuvering simulations were performed based on the captured hydrodynamic derivatives with some pre-assumed propeller and rudder hull interaction parameters with referred to the study of other researchers. Maneuvering comparison of the pusher–barge 11*BP* in shallow water, medium shallow water and deep water conditions was later performed in the study.

2. Ship model

Principal particulars of the pusher and barge in model scale and full-scale used in the research are shown in Table 1. Fig. 1 shows the body plans of the pusher and barge used. During the model experiment, no propeller or rudder was installed on the pusher. In the simulation, the pusher is assumed to be of twin screws and twin rudders, with controllable pitch propeller (CPP) of which diameter (D_P)=1.8 m and revolution=300 rpm. Main engine power is assumed to be 1000 kW. Rudder span is 2.0 m, chord length=2.0 m and area (A_R)=4.0 m^2. The pusher design and specifications are with referred to reference Pfennigstorf (1970).

Rake-barge with ship like design at the bow was used in the study. Bow part of the rake-barge is curved and sharped with water piercing design. In this paper, one pusher and one barge were used as the subject of the study. One rake-barge and a pusher were arranged in-line, named 11*BP*. Table 2 shows the principal dimensions of pusher–barge 11*BP*, where LOA is the length overall of the system, B is the maximum breadth, d is the deepest water draught of the barge, and C_b is the block coefficient with regards to the LOA, B and d of the system.

* Corresponding author. Tel.: +60 7 5534641; fax: +60 7 5566159.
E-mail addresses: koh@fkm.utm.my (K.K. Koh), yasukawa@naoe.hiroshima-u.ac.jp (H. Yasukawa).

0029-8018/$ - see front matter © 2012 Elsevier Ltd. All rights reserved.
doi:10.1016/j.oceaneng.2012.03.002

Table 1
Principal dimensions of the pusher and barge.

Particulars	Pusher		Rake-barge	
	Full-scale	Model	Full-scale	Model
Length overall, LOA (m)	40.00	0.80	60.96	1.22
Length btw. perpendiculars, LBP (m)	39.50	0.79	60.96	1.22
Breadth, B (m)	9.00	0.18	10.67	0.21
Draft, d (m)	2.20	0.044	2.74	0.055
Volume, ∇ (m^3)	494.7	0.00396	1646.2	0.01317
LCB from AP (m)	21.98	0.4395	29.44	0.5888
Block coefficient, C_b	0.633	0.633	0.924	0.924

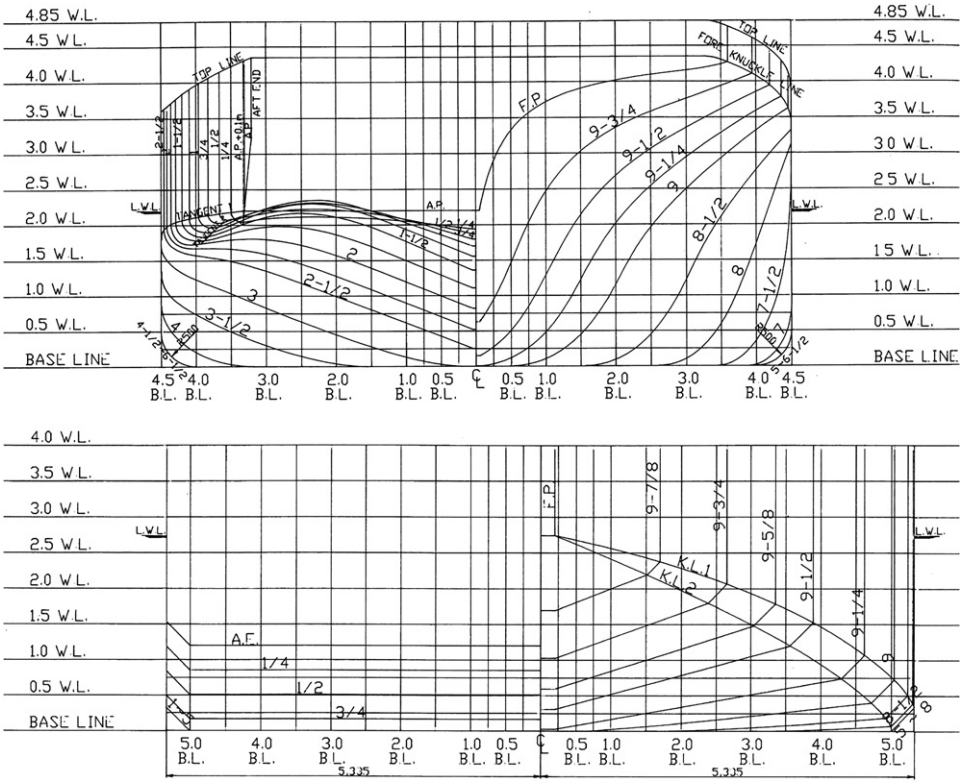

Fig. 1. Body plans of the pusher and the rake-barge.

Table 2
Principal dimensions of the pusher–barge system in full-scale.

Symbol	11*BP*
LOA (m)	100.96
B (m)	10.67
d (m)	2.74
∇ (m^3)	2140.9
LCB from AP (m)	58.47
C_b	0.725

Fig. 2 shows the photo of the actual model of 11*BP* pusher–barge system used in the model experiment. Scale ratio of the model is 1/50.

3. Hydrodynamic derivatives characteristics

3.1. Captive model test

In order to obtain shallow water hydrodynamic derivatives, rotating arm test and constant drift tests were performed at Kyushu University square tank. In the experiments, three different water depth to ship's draught ratios were performed, where $h/d=19.3$ (deep water), 1.5 (medium shallow water) and 1.2 (shallow water). Water was drained from the tank in order to get to the desired water height to model's draught ratio. Model's trim, draught and roll motions were fixed. Model forward speed, $U=0.364$ m/s, is equivalent to full-scale ship's speed of 5 knots. During the experiments, force and moment transducer was used and placed at the midship of the pusher–barge model. Longitudinal force (X_H^*), lateral force (Y_H^*) and yawing moment (N_H) were recorded and non-dimensionalized using the following equations:

$$X_H^{*\prime}, Y_H^{*\prime} = \frac{X_H^*, Y_H^*}{(1/2)\rho\ \mathrm{LOA}\ dU^2} \tag{1}$$

$$N_H' = \frac{N_H}{(1/2)\rho\ \mathrm{LOA}^2\ dU^2} \tag{2}$$

In the equations, ρ is water density, d is model's draught, and U is the forward speed. "$*$" denotes results measured from experiments with virtual mass influence included. No correction was needed for N_H due to virtual mass, hence N_H was used directly in

Fig. 2. Model of pusher–barge 11*BP*.

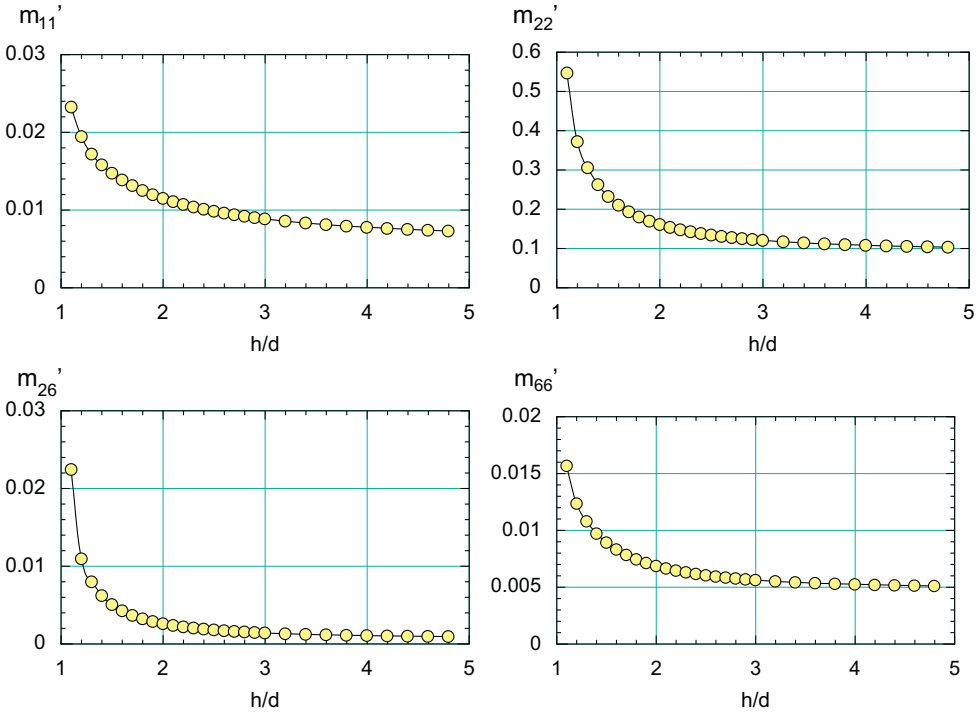

Fig. 3. Shallow water effect on added mass coefficients for 11*BP*.

the equation. Since forces and moment measured from the experiments are having added mass influences included, they must be calculated separately and be excluded when processing the experiment data.

3.2. Added mass coefficients

Added mass coefficients (m'_{11}, m'_{22}, m'_{26}, m'_{66}) in shallow water were calculated using singularity (source/sink) distribution method with the assumption of rigid free-surface. Added mass (m_{11}, m_{22}, m_{26}, m_{66}) were non-dimensionalized using the following equations:

$$m'_{11}, m'_{22} = \frac{m_{11}, m_{22}}{(1/2)\rho\ \mathrm{LOA}^2\ d} \tag{3}$$

$$m'_{26} = \frac{m_{26}}{(1/2)\rho\ \mathrm{LOA}^3\ d} \tag{4}$$

$$m'_{66} = \frac{m_{66}}{(1/2)\rho\ \mathrm{LOA}^4\ d} \tag{5}$$

Fig. 3 shows the shallow water effect on added mass coefficients. From the figure, it is found that added mass coefficients increase significantly when h/d approaches 1.

3.3. Model experiment results of hydrodynamic derivatives

Experimental results of longitudinal force, lateral force and yawing moment in non-dimensional form (X'^{*}_{H}, Y'^{*}_{H}, N'_{H}) are plotted in Fig. 4. Circle, triangle, square, and diamond shapes are data obtained from experiments. Intermediate lines in the figure are fitting using hydrodynamic derivatives obtained from least square method. In general, hydrodynamic derivatives for shallow water, medium shallow water and deep water are having the same plot trend. However, for $h/d=1.2$, at 20° oblique drift angle, Y'^{*}_{H} shows a slowdown. From the experiment data, the second order equation for X'_H with respect to β_m and r' and the third order equation for Y'_H and N'_H were derived, as shown in Eq. (6).

$$\left.\begin{aligned} X'_H &= R'_0\cos^2\beta_m + X'_{\beta\beta}\beta_m^2 + X'_{\beta r}\beta_m r' + X'_{rr}r'^2 \\ Y'_H &= Y'_\beta\beta_m + Y'_r r' + Y'_{\beta\beta\beta}\beta_m^3 + Y'_{\beta\beta r}\beta_m^2 r' + Y'_{\beta rr}\beta_m r'^2 + Y'_{rrr}r'^3 \\ N'_H &= N'_\beta\beta_m + N'_r r' + N'_{\beta\beta\beta}\beta_m^3 + N'_{\beta\beta r}\beta_m^2 r' + N'_{\beta rr}\beta_m r'^2 + N'_{rrr}r'^3 \end{aligned}\right\} \tag{6}$$

In the equation, β_m is the oblique drift angle at midship, r' is the non-dimensional turning rate ($r' \equiv rL/U$), L is the length between perpendiculars, R'_0 is the non-dimensionalized forward resistance ($=-0.0428$) (Koh et al., 2008a), $X'_{\beta\beta}$, Y'_{β}, etc., are the hydrodynamic derivatives. In the previous study (Yasukawa et al., 2007), $Y'_{\beta rr}$ and Y'_{rrr} were neglected due to the limited turning rate in the experiment, making accuracy of higher order of r' was difficult to obtain. However, in this paper, shallow water tests were conducted till $r'=0.7$, fitting in Fig. 4 shows satisfactory results for practical use. From Fig. 4, hydrodynamic derivatives for maneuvering were decided, where for $h/d=19.3$ and 1.5, the obtained hydrodynamic derivatives are good for all drift angle as tested in the study, but for $h/d=1.2$ the obtained hydrodynamic derivatives are limited to drift angle $-5°$ to 15°. Hydrodynamic derivatives

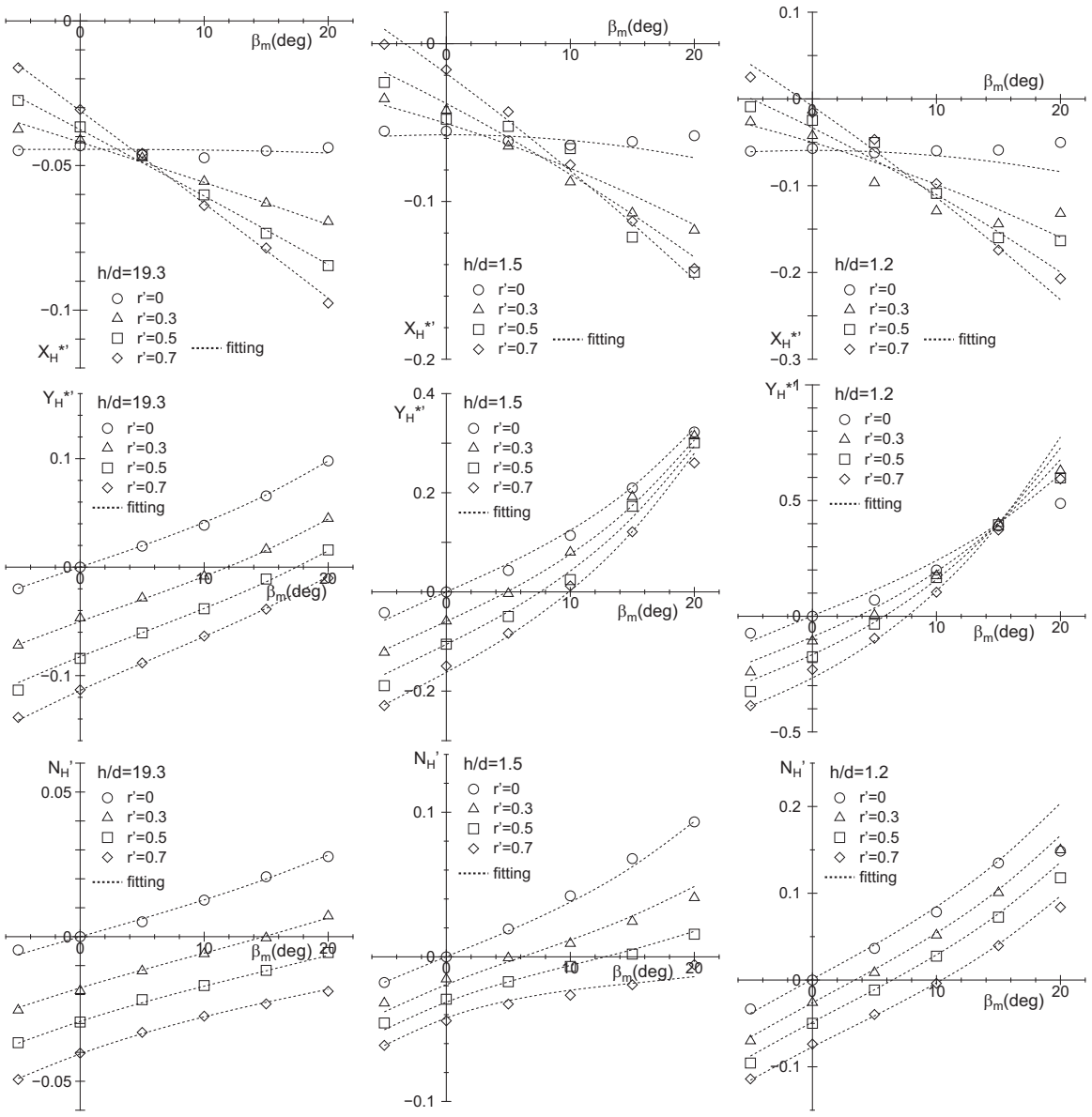

Fig. 4. Hydrodynamic force characteristics for 11*BP* in $h/d=19.3$, 1.5, 1.2.

obtained from the experiments and used in this paper are shown in Table 3. In Table 3, added mass coefficients are shown as well.

3.4. Linear hydrodynamic derivatives and course stability

Linear derivatives obtained from the experiments, Y'_β, Y'_r, N'_β, N'_r, were compared with papers published by other researchers in shallow water studies. Pusher–barge system 11*BP* at different water depth ratios was compared with the linear derivatives of PCC (Yoshimura, 1986), LNGC (Fujino and Ishiguro, 1984), wide beam twin (Yoshimura and Sakurai, 1989), and conventional twin (Yoshimura and Sakurai, 1989). Fig. 5 shows the shallow water effect on linear hydrodynamic derivatives. From the figure, it is found that for $Y'_\beta/Y'_{\beta\text{-}deep}$, pusher–barge 11*BP* is having similar changes of the derivatives from deep to shallow water as LNGC. From $N'_\beta/N'_{\beta\text{-}deep}$ plot, pusher–barge 11*BP* is having similar trend between PCC and wide beam twin vessels. In $Y'_r/Y'_{r\text{-}deep}$ plot, pusher–barge 11*BP* show very high value of $Y'_r/Y'_{r\text{-}deep}$ in medium shallow water and shallow water conditions, and is much higher than the other type of vessels. Plot of $N'_r/N'_{r\text{-}deep}$ shows 11*BP* with significantly lower value of $N'_r/N'_{r\text{-}deep}$ in medium shallow water and shallow water conditions as compared to other vessels.

Course stability index, C, is defined in Eq. (7). Rudder effect is not taken into account in C calculation. Negative value of course stability index in shallow water condition shows that pusher–barge 11*BP* is unstable in course keeping in shallow water.

$$C=\frac{N'_r}{Y'_r-m'-m'_{11}}-\frac{N'_\beta}{Y'_\beta} \tag{7}$$

where m' is the non-dimensionalized mass.

In analyzing the effect of water depth on course stability, changes of $N'_r/(Y'_r-m'-m'_{11})$, N'_β/Y'_β and C versus d/h are plotted as shown in Fig. 6, and their respective values are shown in Table 4. Y_r-m-m_x value was not available from the published paper (Fujino and Ishiguro, 1984), hence LNGC was not included in the course stability analysis. From the figure, for 11*BP*, it is found that at shallow water condition, value of $N'_r/(Y'_r-m'-m'_{11})$ drops when N'_β/Y'_β increases. This resulted in the negative value of C, lead to unstable course keeping ability of the vessel. Wide beam

twin and conventional twin have similar course keeping behavior, while PCC has a different behavior than the rest of the vessels.

4. Turning simulation

4.1. Simulation outline

In order to understand more clearly on the maneuvering behavior of pusher–barge system 11*BP* in different water depths, turning simulation of 20° and 35° rudder angle were carried out. Wind, wave and current effects were not taken into account in the simulations. Propellers and rudders were arranged symmetrically at port and starboard. Pusher–barge 11*BP* has an identical port and starboard turning due to the symmetrical arrangement of hull, propellers and rudders, hence only starboard turn is performed in the simulations. Hydrodynamic derivatives from the previous section are used in the simulations. Details on the simulation calculation are shown in Appendix A.

Table 3
Resistance coefficient, hydrodynamic derivatives and added mass coefficients.

Symbol	$h/d=19.3$	$h/d=1.5$	$h/d=1.2$
$X'_{\beta\beta}$	−0.053	−0.1749	−0.3637
X'_{rr}	0.0272	0.0792	0.1055
$X'_{\beta r}-m'_{22}$	−0.1069	−0.3213	−0.6202
Y'_{β}	0.221	0.6354	1.2375
$Y'_{r}-m'_{11}$	−0.0151	−0.0375	−0.1325
$Y'_{\beta\beta\beta}$	0.4857	2.5353	4.2245
$Y'_{\beta\beta r}$	−0.2268	0.7413	3.6005
$Y'_{\beta rr}$	0.1562	0.286	0.7129
Y'_{rrr}	0.0118	−0.0836	−0.2003
N'_{β}	0.0706	0.1988	0.4435
N'_{r}	−0.0593	−0.0654	−0.0861
$N'_{\beta\beta\beta}$	0.0848	0.5665	1.1277
$N'_{\beta\beta r}$	−0.1407	−0.6547	−0.2249
$N'_{\beta rr}$	0.0358	−0.0528	−0.0561
N'_{rrr}	0.0028	0.0097	−0.0522
m'_{11}	0.0195	0.0148	0.006
m'_{22}	0.3722	0.2325	0.0929
m'_{26}	0.0108	0.005	0.0006
m'_{66}	0.0124	0.0089	0.0049

Propeller, rudder and hull interaction parameters used in the simulations are shown in Table 5 (symbols used in the table are explained in Appendix A). For $h/d=19.3$ deep water case, the parameters used are the same as in papers Yasukawa et al. (2007) and Koh et al. (2008b). For medium shallow water ($h/d=1.5$) and shallow water ($h/d=1.2$) conditions, twin screws wide beam ship as in Yoshimura and Sakurai (1989) was referred. γ_R coefficient is with referred to Yoshimura paper in Yoshimura (1986).

Model resistance obtained from the experiments is having a tendency of decreasing in resistance from deep water to medium shallow water to shallow water conditions. This contradicted with the findings in studies done by other researchers (Millward, 1982, 1991; Hofman, 2000). Hence model resistance of deep water from paper (Koh et al., 2008b) of the same pusher–barge 11*BP* was used. Medium shallow water and shallow water resistances were corrected based on the deep water resistance using Lackenby correction as suggested by ITTC (Lackenby, 1963). Since pusher–barge 11*BP* was moving at slow speed, it falls under sub-critical region for wave resistance correction, no correction for wave resistance is needed (Hofman, 2000).

4.2. Calculation results

Turning trajectories of pusher–barge 11*BP* with 20° and 35° rudder angle starboard turning at different water depths are presented in Figs. 7 and 8. Tactical diameter and advance of the various water depth conditions are presented in Figs. 9 and 10.

Fig. 7 shows turning trajectories of pusher–barge 11*BP* at 20° rudder angle in deep water, medium shallow water and shallow water conditions. From Fig. 7, pusher–barge 11*BP* is having the largest turning trajectory in deep water, followed by medium shallow water, then shallow water conditions. Yasukawa and Kobayashi (1995) and Yoshimura and Sakurai (1989) found that for wide beam vessel, turning circle decreases from deep water to shallow water conditions; whereby for conventional vessel, turning circle increases from deep water to shallow water conditions. Pusher–barge 11*BP* is similar to wide beam vessel in turning

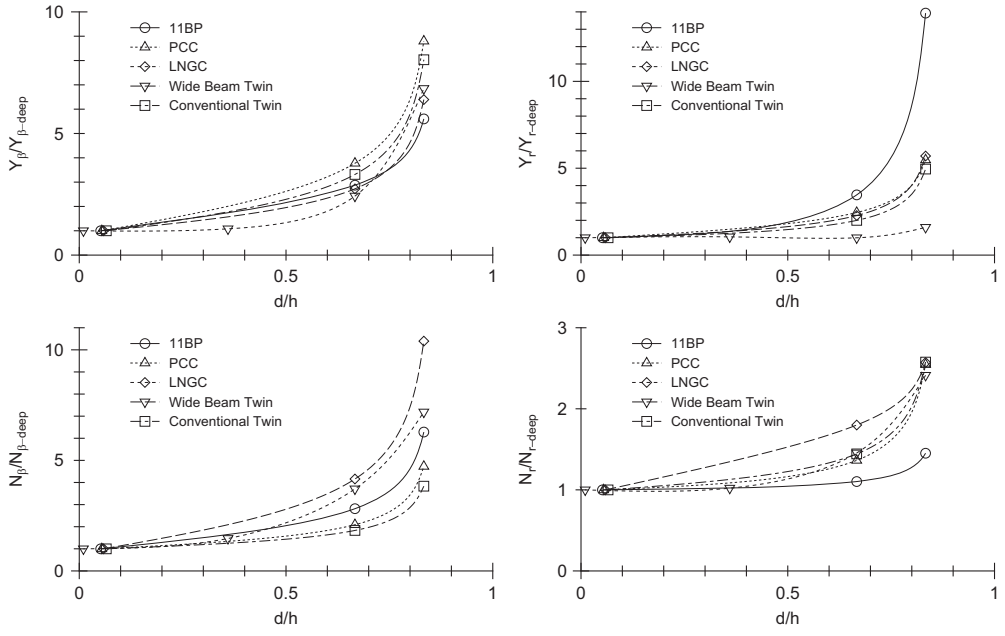

Fig. 5. Shallow water effect on linear derivatives of different ship types.

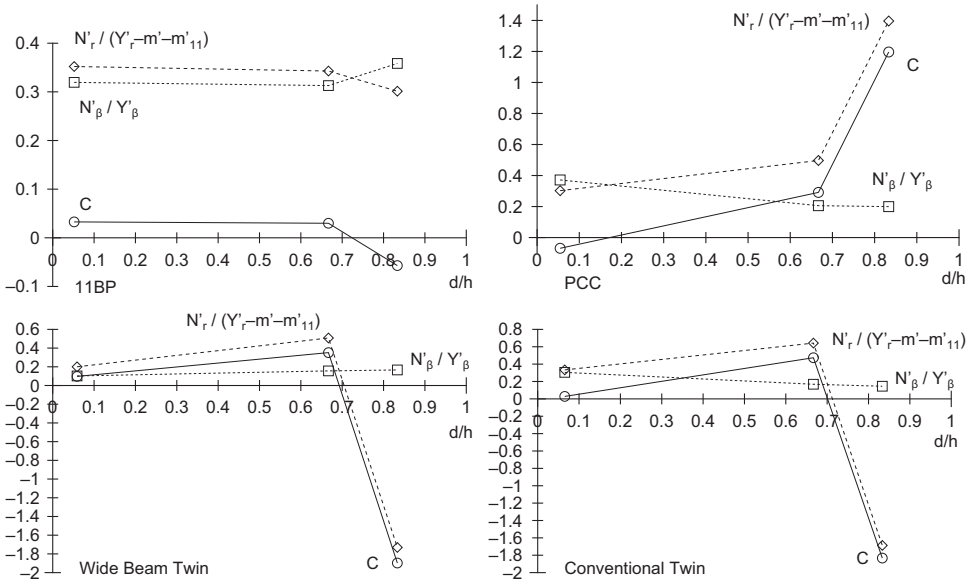

Fig. 6. Course stability index.

Table 4
Resistance coefficient, hydrodynamic derivatives, added mass, and course stability index.

Symbol	$h/d=19.3$	$h/d=1.5$	$h/d=1.2$
$N'_r/(Y'_r-m'-m'_{11})$	0.3521	0.3428	0.3013
N'_β/Y'_β	0.3195	0.3129	0.3584
C	0.0327	0.0299	−0.0571

Table 5
Extra parameters used in the simulation.

Symbol	$h/d=19.3$	$h/d=1.5$	$h/d=1.2$
t	0.164	0.249	0.326
a_H	0.194	0.089	0.418
x'_H	−0.427	−0.249	−0.189
w_{P0}	0.340	0.493	0.576
γ_R	0.230	0.357	0.293
ℓ'_R	−1.033	−0.538	−1.113
ε	0.987	1.189	1.823

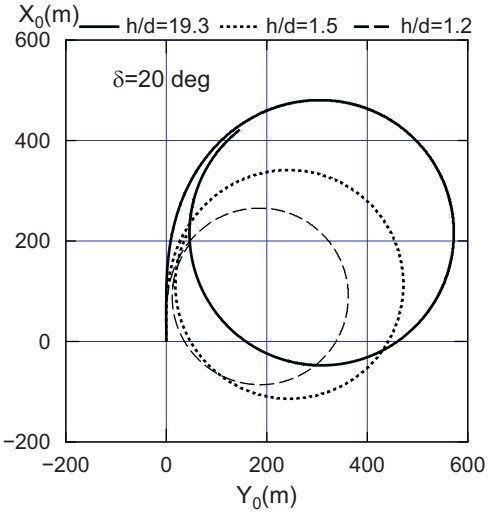

Fig. 7. Turning trajectories ($\delta=20^\circ$).

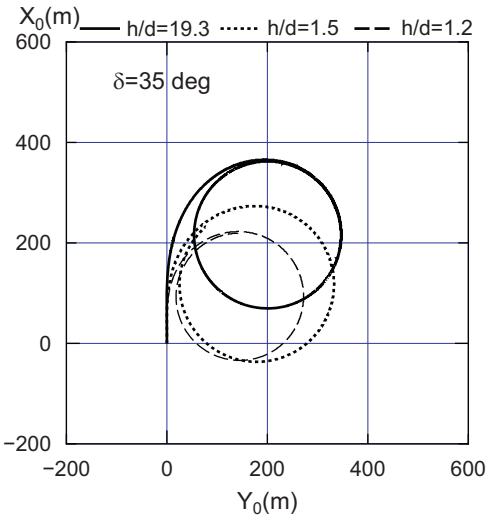

Fig. 8. Turning trajectories ($\delta=35^\circ$).

performance. Fig. 8 shows the turning performance of pusher–barge 11*BP* at rudder angle 35° in deep water, medium shallow water and shallow water conditions, which is similar in trend as compared to rudder angle 25°.

To further analyze the turning simulation results, free running model test that is of similar arrangement as pusher–barge 11*BP* with rudder angle 35° conducted in Indonesian Hydrodynamic Laboratory (IHL) (Yasukawa, 2006) was compared. Results from IHL show that advance increases slightly from $h/d=1.1$ to $h/d=2.0$. For tactical diameter, the value is almost constant throughout the h/d ratio from 1.1 to 2.0. The results match the simulation results of $\delta=35^\circ$ in Fig. 10.

In analyzing the turning behavior of pusher–barge 11*BP* from deep water to medium shallow water to shallow water conditions, rudder force in the three water depth conditions was studied. Fig. 11 shows the rudder force plot in time series for pusher–barge 11*BP* in 20° and 35° rudder angle for deep water, medium shallow water and shallow water conditions. From the figure, it can be seen that pusher–barge 11*BP* in shallow water and medium shallow water conditions have significantly higher rudder force by nearly 100% increment as compared to deep water condition. This resulted

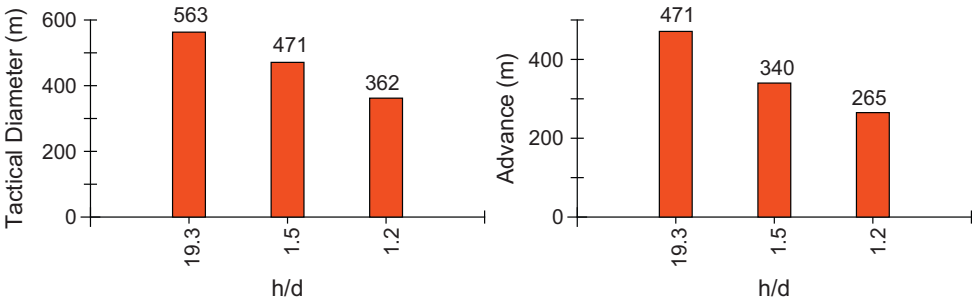

Fig. 9. Tactical diameter and advance distance ($\delta = 20^{\circ}$).

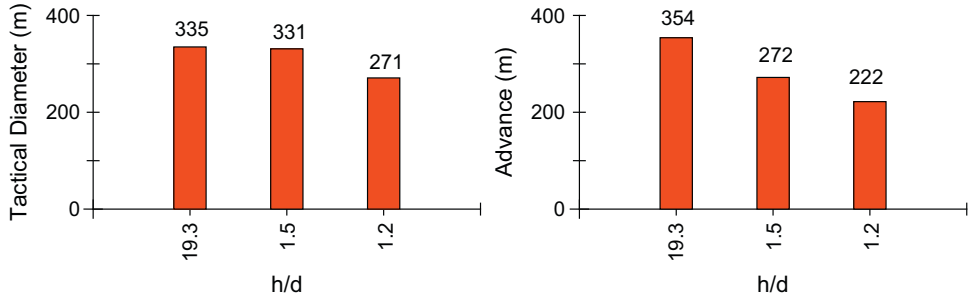

Fig. 10. Tactical diameter and advance distance ($\delta = 35^{\circ}$).

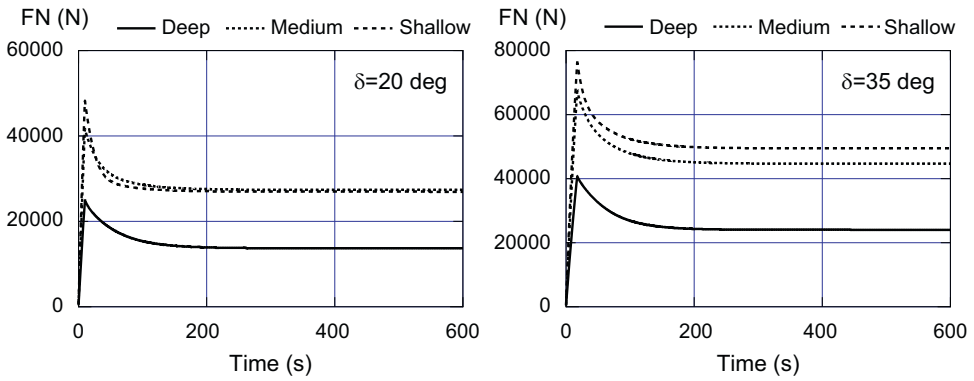

Fig. 11. Rudder force changes in time series for deep, medium shallow water and shallow water conditions.

in better turning performance of pusher barge 11*BP* in medium shallow water and shallow water conditions.

5. Concluding remarks

Pusher–barge system with one pusher and one barge arranged in-line (11*BP*) was studied in this research for three water depth to ship draught ratio conditions ($h/d = 19.3$ (deep water); 1.5 (medium shallow water); and 1.2 (shallow water)). Rotating arm test was carried out in Kyushu University in obtaining the hydrodynamic coefficients of the pusher–barge system in the three water depth to draught ratio conditions. In shallow water condition, pusher–barge 11*BP* is found to have negative value of course stability index (C), which means that the system in unstable in course keeping. In medium shallow water and deep water conditions, pusher–barge 11*BP* has positive but small value of course stability index (0.0299 and 0.0327, respectively), which shows that the pusher–barge system is stable in course keeping but still relatively easy to maneuver when subject to external force.

Simulations were performed on pusher–barge 11*BP* in three water depth to draught ratio conditions on rudder angle 20° and 35°. For rudder angle 20°, pusher–barge 11*BP* turning performance is similar to a wide beam vessel, where turning trajectory decreases from deep to medium shallow water to shallow water conditions. For rudder angle 35°, pusher–barge 11*BP* is having similar turning trend as rudder angle 20°, where the largest turning circle occurs in deep water, followed by medium shallow water and lastly shallow water. Large increment of rudder force in medium shallow water and shallow water conditions was also found in the study.

Free running model test of pusher–barge 11*BP* in comparing with the computer simulation results is suggested to be conducted in future. Different combinations and arrangements of pusher–barge system are also suggested to be tested and simulated for a better understanding of pusher–barge maneuvering characteristics in shallow water condition.

Acknowledgement

The authors want to thank emeritus Professor K. Kijima of Kyushu University for providing the facilities and assistance in conducting the rotating arm test in various water depths conditions.

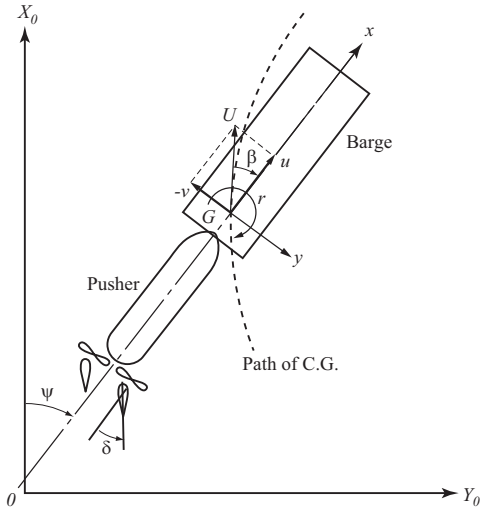

Fig. 12. Coordinate systems.

Appendix A. Maneuvering simulation calculations

Fig. 12 shows the coordinate systems used in the paper. O–$X_0Y_0Z_0$ are the space coordinate system, with X_0Y_0 as to the water surface and Z_0 vertically downwards axis from the water surface. ψ is the angle from X_0 axis to the center of gravity of the ship. G-xyz is the ship's coordinate system, where G is the center of gravity of the ship, x is the forward direction of the ship and y is the lateral direction of the ship. xy forms the water surface where the ship is located and z is the vertical downwards direction from the center of gravity of the ship.

Maneuvering motions of the pusher–barge system (surge, sway, and yaw) are defined in the motion equations shown in Eq. (A.1). In the equation, $\dot{}$ is time based of the respective parameters. The unknown values are: u the forward speed, v the lateral speed and r the turning rate. m is the mass of the ship and I_{zz} is the moment inertia of the ship. m_{11}, m_{22}, m_{26}, and m_{66} are the added mass and added moment of inertia of the pusher–barge system that occur when a ship accelerate or decelerate or in turning motion. On the right hand side of the equation, X is the total forward force, Y is the total lateral force and N is the total yaw moment at the center of gravity of the pusher–barge system.

$$\left.\begin{aligned}&(m+m_{11})\dot{u}-(m+m_{22})vr=X\\&(m+m_{11})ur+(m+m_{22})\dot{v}+m_{26}\dot{r}=Y\\&(I_{zz}+m_{66})\dot{r}+m_{26}\dot{v}=N\end{aligned}\right\} \tag{A.1}$$

X, Y, and N are the forces and moment introduced from hull (H), propeller (P) and rudder (R), which are expressed in Eq. (A.2).

$$\left.\begin{aligned}&X=X_H+X_P+X_R\\&Y=Y_H+Y_R\\&N=N_H+N_R-(Y_H+Y_R)x_G\end{aligned}\right\} \tag{A.2}$$

In model tank test, measurement was done at the midship of the pusher–barge system, while longitudinal force X is unaffected, but lateral force Y and moment N need to be corrected from midship to the center of gravity of the pusher–barge system. The relationship of lateral velocity at midship v_m to the lateral velocity at center gravity of the pusher–barge system v is shown in Eq. (A.3). The midship drift angle β_m is defined in Eq. (A.4).

$$v_m=v-x_G r \tag{A.3}$$

$$\beta_m=\tan^{-1}\left(\frac{-v_m}{u}\right) \tag{A.4}$$

Hydrodynamic force that acts on a hull when a ship makes a diagonal turn is mainly caused by the dynamic pressure of the fluid. If the flow along a hull is to be related to the ship's length, and the displacement of the hull is to be related to the draught of the ship, then the flow and pressure can be related to LOA × d. Hydrodynamic force (X_H,Y_H,N_H) on ship's hull based on the above consideration is shown in Eq. (A.5). In the equation, U is the ship's speed ($U=\sqrt{u^2+v^2}$). X'_H, Y'_H, and N'_H are defined in Eq. (6).

$$\left.\begin{aligned}&X_H=(1/2)\rho\ \mathrm{LOA}\ dU^2X'_H(\beta_m,r')\\&Y_H=(1/2)\rho\ \mathrm{LOA}\ dU^2Y'_H(\beta_m,r')\\&N_H=(1/2)\rho\ \mathrm{LOA}^2\ dU^2N'_H(\beta_m,r')\end{aligned}\right\} \tag{A.5}$$

Propeller at aft of the pusher–barge system only contributing force in the X direction. Total force produced by the propeller as experienced by a ship is defined as

$$X_P=(1-t)\sum T \tag{A.6}$$

where t is the thrust deduction factor and $\sum T$ is the total thrust produces by the propellers (twin screws in this study).

$$T=\rho n_P^2D_P^4K_T(J_P,p) \tag{A.7}$$

In Eq. (A.7) D_P is the propeller diameter, K_T is the thrust coefficient, J_P is the propeller advanced coefficient, and p is the propeller pitch ratio. K_T and J_P are defined in Eqs. (A.8) and (A.9).

$$K_T(J_P,p)=-0.3260pJ_P-0.2005J_P+0.5234p-0.0398 \tag{A.8}$$

$$J_P=\frac{u(1-w_P)}{n_PD_P} \tag{A.9}$$

In Eq. (A.9), w_P is the propeller wake fraction which change accordingly with the drift angle β and also the non-dimensional ship turning rate r'. Hirano's (1980) formula was used in calculating the propeller wake fraction.

$$w_P=w_{P0}\exp[C_1\beta_P^2] \tag{A.10}$$

where w_{P0} is the wake factor during the forward speed of the pusher–barge system, β_P is the drift angle at the propeller position ($\equiv\beta-\ell'_Pr'$), and C_1 is the correction factor. Rudder forces (X_R and Y_R) and moment (N_R) are defined in Eq. (A.11).

$$\left.\begin{aligned}&X_R=-\sum F_N\sin\delta\\&Y_R=-(1+a_H)\sum F_N\cos\delta\\&N_R=-(x_R+a_Hx_H)\sum F_N\cos\delta\end{aligned}\right\} \tag{A.11}$$

where δ is the rudder angle, a_H and x_H are the rudder and hull interaction parameters, and x_R is the x-coordinate point on which the rudder force F_N acts. F_N is defined as below

$$F_N=\tfrac{1}{2}\rho A_RU_R^2f_\alpha\sin\alpha_R \tag{A.12}$$

In the equation, A_R is rudder area and f_α is gradient of the lift coefficient of the rudder. f_α is estimated using Fujii's formula (Fujii and Tuda, 1961). U_R is the flow velocity to the rudder and α_R is the effective rudder in-flow angle

$$U_R=\sqrt{u_R^2+v_R^2} \tag{A.13}$$

$$\alpha_R=\delta-\tan^{-1}\left(\frac{v_R}{u_R}\right) \tag{A.14}$$

In Eq. (A.13), u_R is the water flow speed towards the rudder and v_R is the lateral flow speed after passing the propeller. v_R is calculated using Eq. (A.15) which is related to the rudder location and is influenced by the geometrical inflow angle to the rudder β_R ($\equiv\beta-\ell'_Rr'$), and γ_R is the flow-rectification coefficient to the rudder.

$$v_R=U\gamma_R\beta_R \tag{A.15}$$

u_R is defined using Yoshimura's formula (Yoshimura and Nomoto, 1978)

$$u_R = \frac{\varepsilon u_P}{1-s}\sqrt{1-2(1-\eta\kappa)s+\{1-\eta\kappa(2-\kappa)\}s^2} \quad \text{(A.16)}$$

where s is the propeller slip ratio, η is the ratio of propeller diameter with rudder height, κ is the propeller flow correction factor ($\kappa = 0.6/\varepsilon$ is normally used in deep water case), and ε is the flow coefficient of the rudder with respect to its location.

References

Fujii, H., Tuda, T., 1961. Experimental research on rudder performance (2). J. Soc. Nav. Archit. Jpn. 110, 31–42. (in Japanese).

Fujino, M., Ishiguro, T., 1984. A study of the mathematical model describing Manoevring motions in shallow water. Shallow water effects on rudder-effectiveness parameters. J. Soc. Nav. Archit. Jpn. 156, 180–192. (in Japanese).

Hirano, M., 1980. On the calculation method of ship maneuvering motion at the initial design phase. J. Soc. Nav. Archit. Jpn. 147, 144–153. (in Japanese).

Hofman, M., 2000. Shallow water resistance charts for preliminary vessel design. Int. Shipbuild. Prog. 31 (449), 61–76.

Koh, K.K., Yasukawa, H., Hirata, N., Kose, K., 2008a. Maneuvering simulations of pusher–barge systems. J. Mar. Sci. Technol. 13, 117–126.

Koh, K.K., Yasukawa, H., Hirata, N., Kose, K., 2008b. Hydrodynamic derivatives investigation on unconventionally arranged pusher–barge systems. J. Mar. Sci. Technol. 13, 256–268.

Lackenby, H., 1963. The effect of shallow water on ship speed. Shipbuilder 70 (672).

Millward, A., 1982. The effect of shallow water on the resistance of ship at high sub-critical and super-critical speeds. Trans. R. Inst. Nav. Archit. 124, 175–181.

Millward, A., 1991. A comparison of the effects of restricted water depth on a model and full size planning hull. Trans. R. Inst. Nav. Archit. 133, 237–250.

Pfennigstorf, J., 1970. Handbuch der Werften X Band. Bearb von K Wendel, Schiffahrts-Verlag, Hansa, C Schroedter & Co, Hamburg.

Yasukawa, H. (Eds.), 2006. Study on river transportation by pusher and multi-barge system. The Report of 11th Seminar of JSPS-DGHE Core University Program on Marine Transportation Engineering, Hiroshima University, No 06-1, p. 444.

Yasukawa, H., Hirata, N., Koh, K.K., Punayangkool, K., Kose, K., 2007. Hydrodynamic force characteristics on maneuvering of pusher–barge systems. J. Jpn. Soc. Nav. Archit. Ocean Eng. 5, 133–142. (in Japanese).

Yasukawa, H., Kobayashi, E., 1995. Shallow water model experiments on ship turning performance. In: Mini Symposium on Ship Manoeuvrability, West-Japan Soc. Nav. Archit., 26 May 1995, pp. 71–83.

Yoshimura, Y., 1986. Mathematical model for the manoeuvring ship motion in shallow water. J. Kansai Soc. Nav. Archit. Jpn. 200, 41–51. (in Japanese).

Yoshimura, Y., Nomoto, K., 1978. Modeling of maneuvering behaviour of ships with a propeller idling boosting and reversing. J. Soc. Nav. Archit. Jpn. 144, 57–69. (in Japanese).

Yoshimura, Y., Sakurai, H., 1989. Mathematical model for the manoeuvring ship motion in shallow water 3rd Report. J. Kansai Soc. Nav. Archit. Jpn. 211, 115–126. (in Japanese).